

A simple approach to the joint inversion of seismic body and surface waves applied to the southwest U.S.

Michael West

Department of Physics, New Mexico State University, Las Cruces, New Mexico, USA

Wei Gao and Stephen Grand

Department of Geological Sciences, University of Texas at Austin, Austin, Texas, USA

Received 27 April 2004; revised 2 July 2004; accepted 12 July 2004; published 11 August 2004.

[1] Body and surface wave tomography have complementary strengths when applied to regional-scale studies of the upper mantle. We present a straight-forward technique for their joint inversion which hinges on treating surface waves as horizontally-propagating rays with deep sensitivity kernels. This formulation allows surface wave phase or group measurements to be integrated directly into existing body wave tomography inversions with modest effort. We apply the joint inversion to a synthetic case and to data from the RISTRA project in the southwest U.S. The data variance reductions demonstrate that the joint inversion produces a better fit to the combined dataset, not merely a compromise. For large arrays, this method offers an improvement over augmenting body wave tomography with a one-dimensional model. The joint inversion combines the absolute velocity of a surface wave model with the high resolution afforded by body waves—both qualities that are required to understand regional-scale mantle phenomena. *INDEX TERMS:* 7218 Seismology: Lithosphere and upper mantle; 7255 Seismology: Surface waves and free oscillations; 7294 Seismology: Instruments and techniques; 8109 Tectonophysics: Continental tectonics—extensional (0905); 8180 Tectonophysics: Tomography. **Citation:** West, M., W. Gao, and S. Grand (2004), A simple approach to the joint inversion of seismic body and surface waves applied to the southwest U.S., *Geophys. Res. Lett.*, *31*, L15615, doi:10.1029/2004GL020373.

1. Introduction

[2] Seismic tomography, based on dense regional networks, has proven to be one of the most useful tools for understanding the tectonic regimes which comprise the Earth including continental shields [e.g., *James et al.*, 2001], transforms [e.g., *Thurber et al.*, 2003], continental rifts [e.g., *Gao et al.*, 2004], oceanic plates [e.g., *Forsyth et al.*, 1998a], subduction zones [e.g., *Zhao et al.*, 1992] and mid-ocean ridges [e.g., *Dunn et al.*, 2000]. Models of seismic structure have been used to infer the thickness of the crust and lithosphere, thermal structure, density, magma content and mineralogy—all principal controls on plate tectonics.

[3] The most common type of regional tomography uses teleseismic body wave arrival times to distinguish velocity perturbations beneath the array with upper mantle resolution

as fine as 50 km. Source-side mantle heterogeneities are tacitly assumed to effect the entire array in a similar fashion. To allow for distant structure, it is necessary to remove the mean delay time for each event. This process limits the data to constraining the relative lateral differences in velocity structure. Surface waves offer a different view of the mantle and are widely used to determine mantle shear velocity structure for large aperture investigations. Since surface waves sweep progressively across Earth's surface, absolute velocity can be determined from inter-station travel times. The principal drawback is the limited lateral sensitivity inherent in measuring long-period signals over short baselines. The lateral scale of resolved features for surface waves is frequently an order of magnitude greater than the corresponding body wave tomography.

[4] Because the two types of data are complementary, their joint interpretation is of wide interest. Such joint inversions have been done on a global scale for some time [e.g., *Antolik et al.*, 2003], however, different issues exist for regional-scale joint inversions since body waves are typically demeaned first. The simplest approach is to augment relative tomography results by adding a 1-D structure extracted from a global surface wave model [*Lévêque and Masson*, 1999]. This approach relies optimistically on the local accuracy of the global model. *Allen et al.* [2002] eliminate this uncertainty by deriving an optimum 1-D model specific to the region of study. When the study area is sufficiently large that surface wave velocities change across the array, a 1-D profile is no longer a suitable “background” structure. However, the variation in surface waves can be exploited to refine features within the array, in addition to determining absolute velocity. Here we demonstrate the benefits of a true joint inversion on synthetic and real data. While there are many ways to achieve a joint interpretation of body and surface wave data [e.g., *Van der Lee et al.*, 2003], our goal is to provide a method that builds on the widely-used concepts (and codes) of regional body wave tomography and can be implemented with modest effort.

2. Method

[5] The sensitivity of a body wave traveltime to slowness in an arbitrary gridded model is, in a ray theoretical sense, the ray length in each block (Figure 1). These sensitivities can be inverted with residual travel times to predict models that better fit the data. Phase and group velocities of Rayleigh and Love waves can be measured by one of

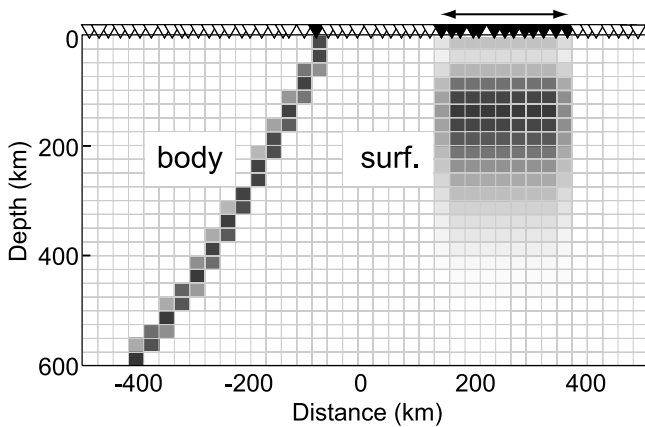


Figure 1. Typical kernels ($\partial t_i/\partial S_j$) for the body and surface waves superimposed on the model parameterization. Seismic stations are shown in white. Body wave kernel is for a teleseismic S wave recorded at the black station. Surface wave kernel is for a 90 s Rayleigh wave recorded across a suite of stations in black. Darker cells have a larger influence on the traveltime.

several techniques. Some include higher modes [e.g., *Nolet, 1975*] and/or multipathing [e.g., *Forsyth et al., 1998b*]. Though a few waveform-based techniques do not require a direct measure of velocities [e.g., *Nolet, 1990*], we assume here that a set of surface wave velocities is extracted from the data.

[6] The crux of our approach is to treat surface wave measurements as travel times between stations. Many surface wave algorithms produce velocity, but the conversion of velocity (and associated errors) into travel time is trivial. Each travel time corresponds to a ray traveling horizontally through a series of blocks in the model. It is the same formulation used for body waves, except that the surface wave “ray” has a sensitivity that is very wide in depth (Figure 1). If the same model space is used to parameterize the surface and body wave problems, then the sensitivity

terms take the same form, $\partial t_i/\partial S_j$, and the surface wave terms can be added as an additional set of ray paths. These terms can be derived from velocity-based 1-D sensitivity kernels as

$$\frac{\partial t_i}{\partial S_j} = l_{i,j} \cdot \frac{\partial C(P_i)}{\partial V_{S_j}} \cdot \left(\frac{V_{S_j}}{C(P_i)} \right)^2 \quad (1)$$

where $C(P_i)$ is the phase (or group) velocity of the i th ray with period P , and $l_{i,j}$ is the horizontal length of the i th ray in the j th model block. $\partial C/\partial V_{S_j}$ are phase (or group) velocity sensitivities to shear velocity integrated over the depth range of block j . The final term converts the sensitivities from velocity to slowness, based on the starting model.

[7] A weighting scheme is necessary to balance the different measurement errors and number of samples in the two datasets. Body wave errors are based on the variance in travel times from clusters of events. Surface wave errors are derived from comparisons of multiple events propagating both directions along the array. The inclusion of surface wave travel time errors is particularly important because they vary greatly with period and station spacing. The simplified representation of surface and body waves as rays introduces error as well [*Spetzler et al., 2002; Tanimoto, 2003*]. Though difficult to quantify, this error has been roughly estimated for the surface waves [*West et al., 2004*]. We invert the data using a weighted damped least squares inversion to incorporate these errors and to allow for regularization.

$$\delta S = [G^T W_b W_e G + \varepsilon^2 W_m]^{-1} G^T W_b W_e \delta t \quad (2)$$

where δt is a vector of travel time residuals, G contains sensitivity kernels ($\partial t_i/\partial S_j$), and δS is the shear wave slowness improvement. W_m contains second derivative smoothing constraints, scaled by ε . The diagonal elements of W_e are σ^{-2} where σ is the standard error of each travel time. The matrices comprise body wave terms on top and surface wave terms on bottom. W_b balances the different

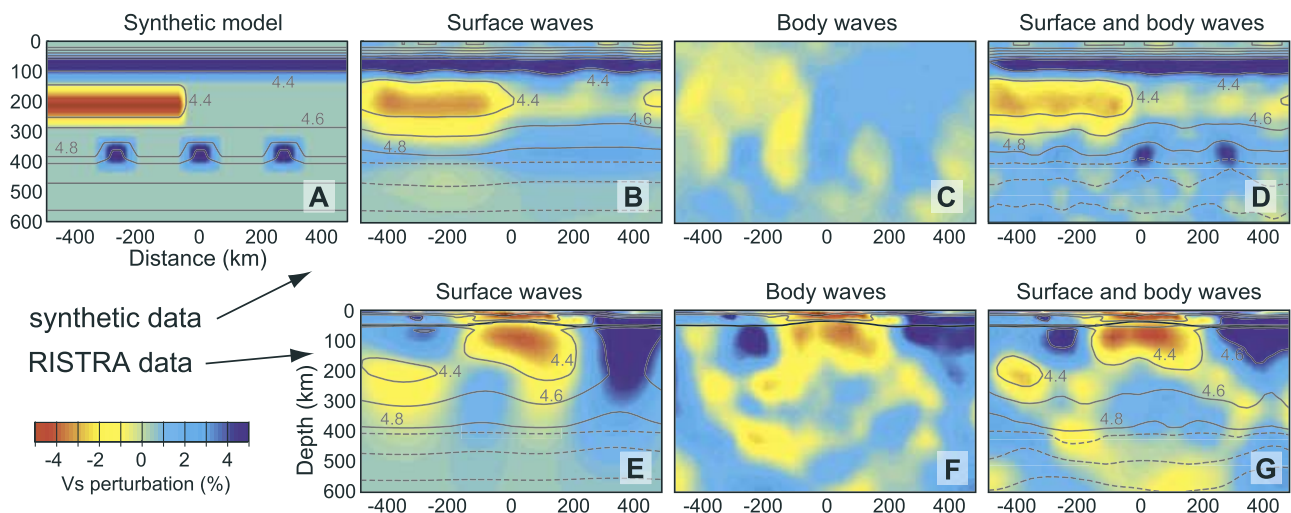


Figure 2. Velocity models derived from synthetic data (top row) and RISTRA data (bottom row). Velocity contours are marked in gray. Color shades represent velocity perturbations relative to 1-D. RISTRA models include an a priori crustal structure used to adjust travel times.

number of body and surface wave observations. We solve equation (2) with a biconjugate gradient approach [Press, 1992], though similar results are achieved using LSQR or a true (non-iterative) inversion. The two types of kernels seek slightly different models. The surface wave terms may seek an offset in the absolute velocity, while the body wave terms seek roughly equal proportions of high and low perturbations. This difference is easily accommodated by using a 1-D starting model optimized to fit the surface waves.

3. Synthetic Tests

[8] We test the approach on a contrived model with challenges for each type of data. Velocities from the AK135 Earth model [Kennett *et al.*, 1995] are sampled onto constant velocity blocks that are 0.25° in width by 25 km in depth. (Figure 1). We add a high velocity sub-crustal layer to mimic a shield-like lithosphere (Figure 2a). Half of the model includes a low velocity asthenospheric channel. Just above the transition zone we include three narrower high velocity features.

[9] We base our body and surface wave coverage on the data and geometry of the recent RISTRA project in the southwestern U.S. S wave coverage includes 2164 S, ScS and SKS arrivals normalized by backazimuth and epicentral distance [Gao *et al.*, 2004]. Relative body wave travel times in the model are perturbed with Gaussian noise ($\sigma = 0.3$ s) based on the observed spread of travel times from event clusters. Fundamental mode Rayleigh wave measurements include 650 inter-station travel times at periods of 30–150 s [West *et al.*, 2004]. We add Gaussian noise as a function of frequency, ranging from 0.25 s (1 σ) at 30 s periods, to 0.95 s for periods of 150 s. We use the data uncertainties to estimate the χ^2 travel time misfit (Table 1). If the errors are uncorrelated and known exactly, χ^2 in the final model should be one to achieve an ideal fit to data without fitting the noise [Constable *et al.*, 1987].

[10] We first invert the body and surface wave data independently (Figures 2b and 2c). The surface wave inversion recovers broad velocity features. The lithosphere and low velocity channel are recovered though smeared in depth owing to the smooth nature of the surface wave sensitivities. The deeper features are too narrow to be resolved though they do elevate velocities across this depth. At these depths, features must be several hundred kilo-

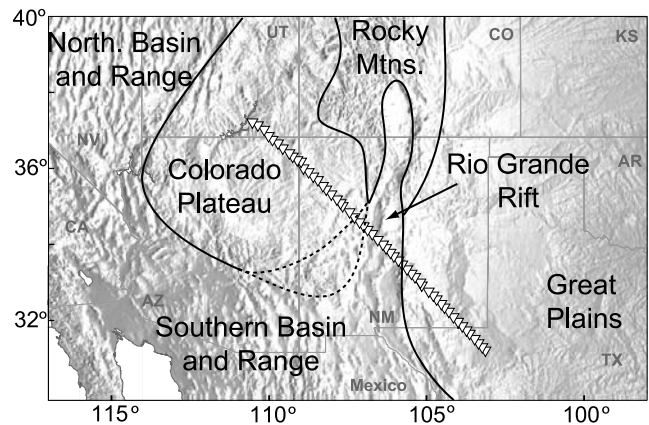


Figure 3. Shaded topographic map of the southwest U.S. White triangles mark stations in the RISTRA deployment. Major tectonic provinces are labeled and outlined in black.

meters wide to overcome the higher measurement error of long period waves. The body wave inversion demonstrates different strengths. The point features above the transition zone are well-resolved. Because the travel times have been demeaned, the anomalies show up as small alternating high and low anomalies. Figure 2c looks worse than typical resolution tests because the mean lateral anomalies are non-zero. However, the peak-to-peak amplitudes are similar to the synthetic model. The low velocity channel is detected, but is smeared drastically in depth. As before, the low velocity channel shows up as fast on the right side of the model and slow on the left. The continuous lithosphere is not resolved since it affects all rays in a similar fashion. The joint inversion returns a much improved model (Figure 2d). If the body wave results had simply been imposed on a 1-D structure, the low velocity channel at 200 km would have been largely missed. The fact that the joint inversion fits the combined dataset better than either independent inversion (Table 1) is evidence that the datasets constrain different portions of the model space.

4. Application to RISTRA Dataset

[11] The RISTRA project typifies modern datasets suited to this methodology (Figure 3). Since it spans the stable North American shield and the tectonic western U.S. [Grand, 1994; Van der Lee and Nolet, 1997], the gross structure cannot be characterized by any single 1-D velocity profile. Yet the Rio Grande Rift provides a narrow target that requires the higher resolving power of body waves. While our linear array cannot constrain all aspects of anisotropy, we note that the sub-vertical S rays and Rayleigh waves respond similarly to radial anisotropy. Shear wave splitting shows a roughly uniform horizontal fast direction across the array [Gök *et al.*, 2003] suggesting that lateral velocity variations can be largely attributed to average velocity, with minimal anisotropic effects. The assumption of uncorrelated error is not true for the real data so we relax the expectation that χ^2 of the travel time misfits will be one. We choose a smoothing value which adequately minimizes both χ^2 and model size (Table 1). An explicit crust and sedimentary basin structure is included based on Wilson *et al.* [2003] and West *et al.* [2004]. The body and

Table 1. Data Fit to Models

	AK135	Surface Wave	Body Wave	Joint Inversion
<i>Synthetic Data</i>				
Misfit (surface) ^a	2.7	1.0	- ^b	1.0
Misfit (body) ^a	7.6	3.8	1.0	1.0
Model size ^{c,d}	0	0.045	0.025	0.045
<i>RISTRA Data</i>				
Misfit (surface) ^a	4.6	1.3	- ^b	1.6
Misfit (body) ^a	8.7	6.3	1.3	1.6
Model size ^c	0	0.081	0.060	0.077

^aMisfit is $\chi^2 = \delta t^T W_c^T \delta t$ using data uncertainties mentioned in text and assuming uncorrelated error.

^bSurface wave velocities cannot be calculated in the body wave model due to the lack of an absolute velocity scale.

^cModel size is rms of $\delta V/V$ with respect to AK135.

^dSize of actual synthetic model is 0.075.

surface wave residuals are adjusted for crustal structure, so we damp the inversion in the top 50 km and include the a priori crust in the final model.

[12] Features in the surface wave image correspond closely to the Colorado Plateau, Rio Grande Rift and Great Plains (Figure 2e). No features are resolved below ~ 350 km. The variation across the array demonstrates the inappropriateness of any single 1-D velocity structure for the region. The body wave image is sharply defined with robust features less than 100 km in width (Figure 2f). A strong low velocity feature is seen in the shallow Earth beneath the Rio Grande Rift. It is roughly 9% slower than similar depths beneath the Great Plains. The high velocity mantle beneath the Great Plains extends to 300 km and appears to continue below 410 km into the transition zone. The shallow mantle beneath the Colorado Plateau is complex suggesting some mix of both high and low velocity regions.

[13] The joint inversion maintains the basic body wave features but with several improvements, including the addition of absolute velocity above ~ 350 km and more lateral continuity of features (Figure 2g). The region beneath the Rio Grande Rift is as slow as 4.25 km/s, indicating solidus temperatures and the existence of partial melt [Cammarano et al., 2003]. Velocities in the adjacent Colorado Plateau and Great Plains provinces reach 4.55 and 4.65 km/s, respectively—typical of cool well-developed lithosphere. Velocities beneath the Great Plains are quite high in the upper 200 km and remain elevated into the transition zone. Beneath the Colorado Plateau they transition below 150 km to a region of low velocity (4.3 km/s) suggesting a warm asthenospheric channel which may help buoy the Colorado plateau at its 2 km elevation [West et al., 2004].

[14] The lateral velocity gradients are the result of thermal variations which could drive small-scale convection. Temperature gradients, a controlling parameter for small-scale convection, are difficult to discern. While the surface waves give an indication of temperature, the model smoothness obscures the scale length of these changes. Conversely, body wave tomography reveals small-scale velocity structures, but cannot be reliably interpreted for temperature because of the non-linear velocity-temperature relationship [Karato, 1993; Cammarano et al., 2003]. The joint inversion provides high resolution and absolute velocity. Extracting the necessary parameters (density, temperature and mineralogy) to make contributions to contemporary issues such as lithospheric composition and small-scale convection require both.

[15] **Acknowledgments.** This manuscript was improved by discussions with and reviews from Tom Hearn, Lapo Boschi, James Ni and an anonymous reviewer. The study would not be possible without the superb data afforded by the RISTRA Team. This work was supported by National Science Foundation grants EAR 9614616, 9706094 and 9707188.

References

Allen, R. M., et al. (2002), Imaging the mantle beneath Iceland using integrated seismological techniques, *J. Geophys. Res.*, *107*(B12), 2325, doi:10.1029/2001JB000595.

- Antolik, M., Y. J. Gu, G. Ekstrom, and A. M. Dziewonski (2003), J362D28: A new joint model of compressional and shear velocity in the Earth's mantle, *Geophys. J. Int.*, *153*, 443–466.
- Cammarano, F., S. Goes, P. Vacher, and D. Giardini (2003), Inferring upper mantle temperatures from seismic velocities, *Phys. Earth Planet. Inter.*, *138*, 197–222.
- Constable, S. C., R. L. Parker, and C. G. Constable (1987), Occam's inversion: A practical algorithm for generating smooth models from electromagnetic sounding data, *Geophysics*, *52*, 289–300.
- Dunn, R. A., D. R. Toomey, and S. C. Solomon (2000), Three-dimensional seismic structure and physical properties of the crust and shallow mantle beneath the East Pacific Rise at 9 degrees 30'N, *J. Geophys. Res.*, *105*, 23,537–23,555.
- Forsyth, D. W., et al. (1998a), Imaging the deep seismic structure beneath a mid-ocean ridge: The MELT experiment, *Science*, *280*, 1215–1218.
- Forsyth, D. W., S. C. Webb, L. M. Dorman, and Y. Shen (1998b), Phase velocities of Rayleigh waves in the MELT experiment on the East Pacific Rise, *Science*, *280*, 1235–1238.
- Gao, W., S. P. Grand, W. S. Baldrige, D. Wilson, M. West, J. F. Ni, and R. Aster (2004), Upper mantle convection beneath the central Rio Grande rift imaged by *P* and *S* wave tomography, *J. Geophys. Res.*, *109*, B03305, doi:10.1029/2003JB002743.
- Gök, R., et al. (2003), Shear wave splitting and mantle flow beneath LA RISTRA, *Geophys. Res. Lett.*, *30*(12), 1614, doi:10.1029/2002GL016616.
- Grand, S. P. (1994), Mantle shear structure beneath the Americas and surrounding oceans, *J. Geophys. Res.*, *99*, 11,591–11,621.
- James, D. E., M. J. Fouch, J. C. VanDecar, and S. van der Lee (2001), Tectospheric structure beneath southern Africa, *Geophys. Res. Lett.*, *28*, 2485–2488.
- Karato, S. (1993), Importance of anelasticity in the interpretation of seismic tomography, *Geophys. Res. Lett.*, *20*, 1623–1626.
- Kennett, B. L. N., E. R. Engdahl, and R. Buland (1995), Constraints on seismic velocities in the Earth from travel times, *Geophys. J. Int.*, *122*, 108–124.
- Lévêque, J.-J., and F. Masson (1999), From ACH tomographic models to absolute velocity models, *Geophys. J. Int.*, *137*, 621–630.
- Nolet, G. (1975), Higher Rayleigh modes in western Europe, *Geophys. Res. Lett.*, *2*, 60–62.
- Nolet, G. (1990), Partitioned waveform inversion and two-dimensional structure under the network of autonomously recording seismographs, *J. Geophys. Res.*, *95*, 8499–8512.
- Press, W. (1992), *Numerical Recipes in C: The Art of Scientific Computing*, 994 pp., Cambridge Univ. Press, New York.
- Spetzler, J., J. Trampert, and R. Snieder (2002), The effect of scattering in surface wave tomography, *Geophys. J. Int.*, *149*, 755–767.
- Tanimoto, T. (2003), Geometrical approach to surface wave finite frequency effects, *Geophys. Res. Lett.*, *30*(19), 1993, doi:10.1029/2003GL017475.
- Thurber, C., S. R. K. Roecker, M. P. L. Gold, and K. Rittger (2003), Earthquake locations and three-dimensional fault zone structure along the creeping section of the San Andreas fault near Parkfield, CA: Preparing for SAFOD, *Geophys. Res. Lett.*, *30*(3), 1112, doi:10.1029/2002GL016004.
- Van der Lee, S., and G. Nolet (1997), Upper mantle *S* velocity structure of North America, *J. Geophys. Res.*, *102*, 22,815–22,838.
- Van der Lee, S., J. VanDecar, M. Fouch, and D. James (2003), Upper mantle structure beneath southern Africa from multidisciplinary constraints, *Geophys. Res. Abstr.*, *5*, Abstract 05918.
- West, M., J. Ni, W. S. Baldrige, D. Wilson, R. Aster, W. Gao, and S. Grand (2004), Crust and upper mantle shear-wave structure of the southwest United States: Implications for rifting and support for high elevation, *J. Geophys. Res.*, *109*, B03309, doi:10.1029/2003JB002575.
- Wilson, D., R. Aster, W. S. Baldrige, W. Gao, R. Gök, S. Grand, J. Ni, E. Sandvol, S. Semken, and M. West (2003), Imaging crust and upper mantle seismic structure in the southwestern United States using teleseismic receiver functions, *Leading Edge*, *22*, 232–237.
- Zhao, D., A. Hasegawa, and S. Horiuchi (1992), Tomographic imaging of *P* and *S* wave velocity structure beneath northeastern Japan, *J. Geophys. Res.*, *97*, 19,909–19,928.

W. Gao and S. Grand, Department of Geological Sciences, University of Texas at Austin, Austin, TX, USA.

M. West, Department of Physics, New Mexico State University, Las Cruces, NM 88003, USA. (west@nmsu.edu)